Impacts of Automated Mobility-on-Demand on traffic dynamics, energy and emissions: A case study of Singapore

Oh, Simon; Lentzakis, Antonis F.; Seshadri, Ravi; Ben-Akiva, Moshe

Published in:
Simulation Modelling Practice and Theory

Link to article, DOI:
10.1016/j.simpat.2021.102327

Publication date:
2021

Document Version
Peer reviewed version

Journal Pre-proof

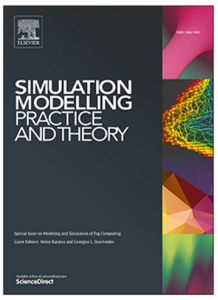

Impacts of Automated Mobility-on-Demand on traffic dynamics, energy and emissions: A case study of Singapore

Simon Oh, Antonis F. Lentzakis, Ravi Seshadri, Moshe Ben-Akiva

PII: S1569-190X(21)00045-9
DOI: https://doi.org/10.1016/j.simpat.2021.102327
Reference: SIMPAT 102327

To appear in: *Simulation Modelling Practice and Theory*

Received date : 6 November 2020
Revised date : 19 March 2021
Accepted date : 26 March 2021

Please cite this article as: S. Oh, A.F. Lentzakis, R. Seshadri et al., Impacts of Automated Mobility-on-Demand on traffic dynamics, energy and emissions: A case study of Singapore, *Simulation Modelling Practice and Theory* (2021), doi: https://doi.org/10.1016/j.simpat.2021.102327.

Impacts of Automated Mobility-on-Demand on Traffic Dynamics, Energy and Emissions: A Case Study of Singapore

Simon Oh[a,d], Antonis F. Lentzakis[a], Ravi Seshadri[c], Moshe Ben-Akiva[b]

[a]*Future Urban Mobility, Singapore-MIT Alliance for Research and Technology (SMART) 1 CREATE Way, #09-02 CREATE Tower, Singapore 138602*
[b]*Department of Civil and Environmental Engineering, Massachusetts Institute of Technology (MIT), Cambridge, MA 02139, United States*
[c]*Department of Technology, Management and Economics, Technical University of Denmark (DTU), 2800 Kgs. Lyngby, Denmark*
[d]*Department of Data Science, Sejong University, 209 Neungdong-ro, Gwangjin-gu, Seoul, Republic of Korea*

Abstract

Technological advancements have focused increasing attention on Automated Mobility-on-Demand (AMOD) as a promising solution that may improve future urban mobility. During the last decade, extensive research has been conducted on the design and evaluation of AMOD systems using simulation models. This paper adds to this growing body of literature by investigating the network impacts of AMOD through high-fidelity activity- and agent-based traffic simulation, including detailed models of AMOD fleet operations. Through scenario simulations of the entire island of Singapore, we explore network traffic dynamics by employing the concept of the Macroscopic Fundamental Diagram (MFD). Taking into account the spatial variability of density, we are able to capture the hysteresis loops, which inevitably form in a network of this size. Model estimation results at both the vehicle and passenger flow level are documented. Environmental impacts including energy and emissions are also discussed. Findings from the case study of Singapore suggest that the introduction of AMOD may bring about significant impacts on network performance in terms of increased VKT, additional travel delay and energy consumption, while reducing vehicle emissions, with respect to the baseline. Despite the increase in network congestion, production of passenger flows remains relatively unchanged.

Keywords: Automated Mobility-on-Demand (AMOD), Agent-based Simulation, Macroscopic Fundamental Diagram (MFD), Multimodality

1. Introduction

Recent technological advancements are changing the way we view urban mobility systems and are set to bring about a host of opportunities to improve mobility, accessibility, and livability. This is evident from the advent of transportation networking companies (TNC) and ride-sourcing services, hereafter termed Mobility-on-Demand (MOD). TNCs are rapidly embracing new business models of shared mobility, on-demand ride-hailing and seamless multimodality, by employing a multi-sided business platform which attracts both drivers and customers (passengers). App-based MOD services have become an entrenched mobility option penetrating 7-8% of the market, generating 44 billion USD of worldwide revenue

in 2017 (OECD, 2018), and are projected to reach a market penetration rate of 13% with double the revenue within five years (Statista, 2017). The main factors to which the large adoption rates can be attributed are respondents' satisfaction with low waiting and travel times, ease-of-use, and the convenience of smartphone-based services (Rayle et al., 2016).

The potential of integrating autonomous vehicle (AV) technology and ride-sourcing platforms, as part of AV-based on-demand shared-ride services, hereafter termed Automated Mobility-on-Demand (AMOD), has been well recognized by major technology companies. Significant progress has been made in AV technology itself by the traditional automotive industry as well as the emerging AV software platform companies, including Nvidia Drive AGX, Aptiv (formerly Delphi Connection Systems), Waymo (formerly Google Self Driving Car project). Technology companies have been running trials on AV-based mobility services, e.g., Waymo has accumulated more than 10 million miles of on-road testing from 2009 to 2018. Some major players are contributing to the realization of AMOD services by entering into partnerships with traditional car-makers and TNCs, e.g. the Early Ride Program by Waymo with self-driving Chrysler cars in Phoenix, the first commercial service by Aptiv which takes advantage of the ride-hailing network of Lyft with an autonomous fleet of BMW cars in Las Vegas.

Recent market research (Jadhav, 2018) projects the growth of the global autonomous mobility market to increase from 5 billion USD (in 2019) to 556 billion USD (in 2026) with foreseeable benefits including improved safety (given the fact that 94% of accidents are caused by human factors), higher transportation network throughput, improved efficiency (with centralized fleet operation), more affordable services (due to competitive cost structures), as well as other long-term benefits on urbanization. However, these benefits are as of yet far from guaranteed, because of economic and social barriers (Fagnant and Kockelman (2015)), large uncertainty on the cost and pricing of AMOD (Bösch et al. (2018)), and potential adverse effects of AMOD on existing transportation systems, such as induced demand, cannibalization of transit, congestion, increased Vehicle-Kilometers-Traveled (VKT), and empty trips involving dead heading (Simoni et al. (2019); Hörl et al. (2019); Zhang et al. (2018)), as has already been observed with MOD services (Laris). For this reason, a recent white paper (Katherine Kortum, 2018) also points out the importance of studying the design of AMOD systems (involving fleet management and operation, supply of infrastructure for charging and parking) and their impacts on transportation (including system capacity, VKT, transit, travel behavior and land use patterns). Regarding future challenges, the standing committee on traffic flow theory and characteristics (TFTC) suggests specific directions over four primary areas: simulation, connected and automated vehicle technologies, network-wide modeling, and multimodality (Ahn et al. (2019)).

In this respect, this paper studies the potential network impacts of AMOD using an agent- and activity-based traffic simulation platform. Demand is modeled using an activity-based model system (ABM), that draws on stated preferences data from a smartphone-based survey in Singapore. Supply is modeled using an on-demand mobility service controller (that replicates the operations of MOD/AMOD fleets involving assignment and rebalancing of service vehicles) integrated within a mesoscopic multimodal network simulator. Interactions between demand and supply are explicitly modeled. Through scenario simulations of the entire network of Singapore, we contribute to the literature on AMOD, by employing network-wide Macroscopic Fundamental Diagrams (hereafter termed as MFDs) to explore congestion pat-

terns over the entire network. In order to examine the impact of introducing AMOD services on existing multimodal networks, we take inspiration from past literature on generalization (e.g. Ramezani et al. (2015)) and extension of the MFD concept (e.g. Geroliminis et al. (2014)).

2. Past Research

2.1. AMOD System Design and Evaluation

Extensive research, employing simulation-based optimization methods, has endeavoured to analyze the impact of AMOD services on transportation networks. Initial studies examined the potential of AMOD services using queuing theory and network models. Spieser et al. (2014) estimated the AMOD fleet size required to serve all existing private vehicle trips in Singapore and concluded that fewer vehicles are required to serve existing demand with reasonable waiting times. Along similar lines, Burns et al. (2015) analyzed travel patterns, cost estimates, and vehicle requirements for different network configurations corresponding to mid-sized, low-density, and densely-populated urban areas.

Researchers have also addressed the deployment and operations of on-demand services and proposed novel vehicle assignment and rebalancing strategies to efficiently deal with spatio-temporal variations in demand. Linear and integer programming approaches were utilized for the minimization of vehicle rebalancing while maintaining vehicle availability over the network (Pavone et al. (2011), Zhang and Pavone (2016)). Similarly, Zachariah et al. (2014) solved a rebalancing assignment problem of AV taxis in New Jersey by minimizing the number of empty vehicles on the network. Researchers have also proposed solutions to the fleet sizing problem using the concept of shareability networks and –using the New York taxicab dataset– have shown a significant reduction in the cumulative trip length (Santi et al. (2014)) and required fleet size to accommodate existing demand (Alonso-Mora et al. (2017); Vazifeh et al. (2018)). Hyland and Mahmassani (2018) employed an agent-based simulation, which uses a mathematical programming solver to compare a variety of heuristic and optimization-based assignments in grid networks. Presenting a case study with Chicago taxi demand data, they suggest that 'sophisticated' assignment algorithms are able to serve more incoming requests with limited fleet size and result in fewer empty vehicles within the fleet.

Regarding the effects of AMOD services, Martinez and Viegas (2017), using agent-based simulations, reported the potential reduction of vehicle population, travel volume, and parking spaces and increased fleet mileage in Lisbon, Portugal. Similar findings have also been reported in Fagnant and Kockelman (2014), who examined AMOD service impacts with a portion of existing trips (taken from NHTS, 2009) in a synthetic city similar to Austin, Texas. Their results showed that shared AVs (hereafter termed as SAVs) can fulfill the vehicle needs of nearly 12 privately owned cars, serve 31 to 41 requests per day, and reduce the required parking spaces by 11 per service vehicle. However, these studies fail to capture network congestion effects, as well as the interactions between demand and supply.

Recent studies have addressed the aforementioned shortcomings using agent-based traffic simulations. Boesch et al. (2016) determined the fleet sizes required to satisfy different levels of demand in the greater Zurich area, Switzerland, using the multi-agent transport simulation software MATSim (Horni et al. (2016)) and reported that a significant reduction

in the vehicle population can be achieved when introducing an AMOD service (that can fulfill requests within a waiting time of 10 minutes, similar to previous literature). Bischoff and Maciejewski (2016) obtained similar results on the replacement of private trips, for the city of Berlin, by solving the dynamic vehicle routing problem (DVRP) with MATSim. Maciejewski and Bischoff (2016) investigated congestion effects of AV taxis with travel time and delay ratios for scaled-down scenarios over different settings (of replacement rates, fleet sizes, and road capacity levels) and suggested that large fleets may aggravate congestion because of unoccupied trips, assuming there is no road capacity improvement by automation. Further, simulation scenarios of Zurich from Hörl et al. (2019) tested different AMOD fleet operational policies using the daily travel patterns extracted from a synthetic Swiss population (which generated around 360k trips for AMOD). The study reported that –using a feedforward fluidic rebalancing algorithm– a fleet size of 7,000 vehicles was able to serve 90% of requests within 5 minutes, and further examined the cost implications of AMOD services based on Bösch et al. (2018). From a recent case study (Segui-Gasco et al. (2019)) in Greenwich, London, UK, the authors integrated a fleet simulation software called IMSim to MATSim in order to evaluate different configurations of vehicle specifications, fleet sizes, parking and charging infrastructure and service criteria from traveler, operator, and city's perspectives. The authors indicated the negative effects of AMOD, whereby AMOD fleet vehicles come to have additional travel distances, which may result in added congestion, thus emphasizing the need for future research to conduct more detailed investigations. In order to explicitly consider demand-supply interactions, Azevedo et al. (2016) analyzed the sensitivity of AMOD supply (i.e. fleet sizes, parking configurations) on travel behavior (i.e. mode shares, routes, and destination choices), and more recently, Basu et al. (2018) investigated the potential of AMOD services to substitute mass transit, using an agent- and activity-based simulation platform.

Despite the growing body of literature on AMOD systems, several limitations remain:

(i) Simplified abstraction of the urban network including grid type networks (Fagnant and Kockelman (2014)), Euclidean planes (Spieser et al. (2014)), quasi-dynamic grid-based networks (Zhang and Pavone (2015); Martinez and Viegas (2017); Fagnant and Kockelman (2018)), synthetic grids (Hyland and Mahmassani (2018)), prototypical cities (Basu et al. (2018))

(ii) Coarse-grained simulation models where approximations are made that employ static travel times without using detailed models of network congestion (Spieser et al. (2014); Alonso-Mora et al. (2017); Fagnant and Kockelman (2018); Farhan and Chen (2018); Chen et al. (2016); Burns et al. (2015); Zhang and Pavone (2016); Boesch et al. (2016))

(iii) Substituting a proportion of existing private trips with AMOD and limited modeling of behavioral preferences towards AMOD (Burns et al. (2015); Boesch et al. (2016); Zhang and Pavone (2016); Maciejewski and Bischoff (2016); Bischoff and Maciejewski (2016); Hörl et al. (2019)).

To overcome these limitations, recent studies have started to integrate on-demand service simulators with a traffic simulator (i.e. Segui-Gasco et al. (2019); Oh et al. (2020b,a)) to capture future impacts of AMOD on demand and supply. However, an analysis of network traffic dynamics has, to the best of our knowledge, not been conducted on large-scale urban

networks, and consequently, the understanding of the network effects of AMOD still warrants investigation.

2.2. Network-wide Traffic Modeling

A recent trend for capturing congestion patterns of urban areas is modeling and analyzing network traffic dynamics at the urban-scale, utilizing the MFD concept. In the past decade, the spatial scale of traffic modeling has been extended to the network level, whereby aggregated traffic dynamics are described collectively over the urban area. Initial studies on macroscopic relationships dating back to the 1960s, determined the optimum density necessary for sustaining maximum flow rate in a given area (Smeed (1967); Godfrey (1969)). Following that, Herman and Prigogine (1979) proposed a two-fluid model that models the relationship between average vehicular speed and density, later verified by simulation (Mahmassani et al. (1987)). The concept of the MFD was formalized by assuming a homogeneous congestion distribution over an urban area (Daganzo (2007)) and empirically evidenced by the well-defined macroscopic relationship between network production (i.e. average flow, trip completion rate) and accumulation (average density, total vehicles on the network), in a study of Yokohama, Japan (Geroliminis and Daganzo (2008)). The existence of MFDs have since been verified and reproduced for other cities all over the world: Toulouse, France (Buisson and Ladier (2009)), Zurich, Switzerland (Ambühl et al. (2017); Loder et al. (2017)), Rome, Italy (Bazzani et al. (2011)), Sendai, Japan (WADA et al. (2015)), Shenzhen, China (Ji et al. (2014)), Brisbane, Australia (Tsubota et al. (2014)), Minnesota, USA (Geroliminis and Sun (2011)), Amsterdam, Netherlands (Knoop and Hoogendoorn (2013)), Lyon, France (Mariotte (2018)).

The MFD concept has been employed in the implementation of large-scale traffic control measures by reducing vehicle accumulation to its critical level so as to mitigate overall congestion. It includes perimeter control, whereby metering of the number of vehicles into a specific "protected" region takes place (Daganzo (2007); Haddad and Geroliminis (2012); Haddad et al. (2013); Keyvan-Ekbatani et al. (2012); Ramezani et al. (2015); Geroliminis et al. (2012); Kouvelas et al. (2017); Kim et al. (2018)), pricing affecting travel behavior on mode and destination choice (Geroliminis and Levinson (2009); Gonzales and Daganzo (2012); Zheng et al. (2012); Simoni et al. (2015); Zheng and Geroliminis (2016)), route guidance (Yildirimoglu et al. (2015); Lentzakis et al. (2018)), space allocation (Zheng and Geroliminis (2013)), and parking (Leclercq et al. (2017)).

To estimate the MFD, researchers have utilized both analytical and experimental approaches. Daganzo and Geroliminis (2008) analytically presented the 'cuts method' based on variational theory by determining the different upper bounds on the MFD plane. Later, Leclercq and Geroliminis (2013) utilized this approach in estimating the MFD in simple networks with different routes, and Laval and Castrillón (2015) proposed a stochastic approximation method to estimate the MFD of an urban corridor based on variational theory. Studies employing experimental approaches estimated the flow and density with sensor data observed based on Eulerian (Shoufeng et al. (2013)) and Lagrangian (Nagle and Gayah (2013)) approaches. Readers can refer to Leclercq et al. (2014) for more details.

The shape of MFDs can be affected by several factors including network supply (e.g. geometric features, signal timings, road capacity, heterogeneity of congestion) and demand (e.g. route choice, detouring, OD flows). Buisson and Ladier (2009) attributed the loop-like

hysteresis shape of the MFD to the local heterogeneity of sensor distribution over the network, network composition involving road types and spatial distribution of demand and local congestion, and were the first to relax the homogeneity conditions of the MFD described in earlier studies (Geroliminis and Daganzo (2008); Geroliminis et al. (2007)). This hysteresis phenomenon has been repeatedly observed or reproduced from further studies on both empirical data and simulation data (Mazloumian et al. (2010); Gayah and Daganzo (2011), Daganzo et al. (2011), Geroliminis and Sun (2011), Mahmassani et al. (2013), Mühlich et al. (2014), Saeedmanesh and Geroliminis (2015)) showing different average flow rates during the onset and dissipation of congestion. In addition, the degree of spatial variation of network occupancy has been used to explain the size of hysteresis (Saberi and Mahmassani (2012); Saberi et al. (2014)). To incorporate the spatial variation into the MFD modeling framework, Knoop et al. (2015) generalized the MFD (GMFD), describing the relation between average flow with average density and density heterogeneity. The authors explained the occurrence of hysteresis as a result of nucleation effects and demonstrated the performance loss due to spatial heterogeneity. Knoop and Hoogendoorn (2013) predicted network production by formulating the GMFD with both non-parametrized and parameterized forms. Ramezani et al. (2015) also integrated the dynamics of heterogeneity into the aggregated model for subregion-based MFDs and their perimeter control.

The effect of route choice behavior on the scatter of MFD has been explored by many studies (Yildirimoglu et al. (2015); Leclercq and Geroliminis (2013); Gayah and Daganzo (2011); Gayah et al. (2014)). Leclercq and Geroliminis (2013) posited that the scatter of MFD is affected by route choices and (uneven/inconsistent) distribution of congestion. Gayah and Daganzo (2011) showed in simulations that hysteresis loops can be reduced in size through adaptive route choice with respect to congestion. Also, demand patterns (derived from route choice) have been identified as a factor leading to bifurcation at the high density part of MFD (Leclercq et al. (2015); Shim et al. (2019)) and network instability (Daganzo et al. (2011); Mahmassani et al. (2013)).

Recent studies have extended the MFD into three dimensions to explain the passenger and vehicle flow in multimodal networks. One notable study by Geroliminis et al. (2014) suggests a three-dimensional MFD capturing the performance of bi-modal networks by relating the accumulation of cars and buses with the vehicle and passenger flow, which they call 3D-vMFD, 3D-pMFD respectively. Ampountolas et al. (2017) proposed a solution to the perimeter control problem by controlling the vehicle composition of bi-modal traffic. Loder et al. (2017) was able to derive 3D-MFDs using data from loop detectors and public transit in the city of Zurich. The authors estimated the 3D model using a linear relationship between vehicle density and speed for each mode and measured the effect of vehicle accumulation on the speed of cars and buses. These studies suggested negative marginal effects for additional vehicles (higher for bus than car) on network speed. Paipuri and Leclercq (2020) simulated three different MFD-based models (accumulation-, trip- and delay accumulation-based approach) over different traffic states considering the 3D-MFD concept for a grid network with dedicated bus lanes. The authors highlighted the importance of segregated 3D-MFDs to accurately resolve traffic dynamics.

In summary, extensive research has been conducted in regard to both AMOD system design and the modeling of network-wide traffic. However, despite the extensive literature, the network impact of AMOD services, with respect to congestion, still warrants further

investigation, particularly in large-scale urban networks. This paper attempts to fill the gap between these two areas by explicitly investigating network-wide congestion effects from the MFD perspective through a high-fidelity agent-based traffic simulation platform. Following this section, Section 3 presents the agent-based simulation framework and the formulation of the MFD for the simulation scenarios described in Section 4. Then, in Section 5 we analyze and estimate the network-wide MFD (Section 5.1), followed by, Section 5.2, which discusses the impacts of congestion from the standpoint of traveler, operator, and planner. Finally, Section 6 presents conclusions, as well as future research directions.

3. Methodology

3.1. Simulation Framework

We utilize the high-fidelity activity- and agent-based simulation platform (*SimMobility* (Adnan et al. (2016)) to model daily network-wide trips, for all agents in an urban area. *SimMobility* is comprised of three primary components operating at different temporal scales, the Short-term, Mid-term and Long-term. In this study, we will primarily make use of *SimMobility Mid-term* (Lu et al. (2015)), which models daily activity and travel demand and simulates multimodal network performance at a mesoscopic level. The Mid-term is composed of three modules, the *Pre-day*, *Within-day*, and *Supply*, as shown in Figure 1.

The *Pre-day* module is a system of hierarchical discrete choice models (logit and nested-logit) and simulates the daily activity patterns of individuals through an activity-based model system (*ABM*) (Ben-Akiva et al., 1996). The pre-day model system consists of three levels:

- The day pattern level generates a list of tours and availability of intermediate stops for each activity type (work, education, shopping, and others).
- The tour level describes the details for each tour including destination, travel mode, time of day (arrival time and departure time) and occurrence of work-based sub-tours.
- The intermediate stop level generates the intermediate stops for each tour and predicts the details of the secondary activities (including destination, mode, etc).

The *Pre-day* model system provides the daily activity schedule (*DAS*) – a detailed description of individual activity and mobility patterns, including arrival/departure time, destination (at zonal level), and travel mode for each trip/tour. Interested readers can find more details of the *Pre-day* model in Siyu (2015).

At the *Within-day* level, the pre-day activity schedule is transformed into actions by performing departure time choice, route choice and within-day re-scheduling of individual trips (Ben-Akiva, 2010). Following this, the *Supply* module simulates network dynamics using macroscopic traffic flow relationships (speed-density models) combined with deterministic queuing models, as well as public transit operations through bus and rail controllers that dispatch vehicles (frequency/headway-based operation), monitor the vehicle occupancy, and determine the dwell time at stops/stations. The *Supply* model also includes a *Smart Mobility Service (SMS) controller* that replicates the operations of an on-demand ride-sharing mobility service (Basu et al. (2018)). For trips that require on-demand services (MOD, AMOD), the agent (passenger) sends a ride request to the controller with pertinent details, including

service type (single, shared), and origin/destination for Pick-Up/Drop-Off (PUDO). Subsequently, the controller accommodates the client's request by assigning and dispatching the service vehicle from the available vehicle list in the fleet which satisfies constraints on:

(i) new passenger's minimum waiting time (wt_{min})

(ii) existing passenger's additional travel time due to detours (tt_{ad})

(iii) the number of seats available in the service vehicle (C_v).

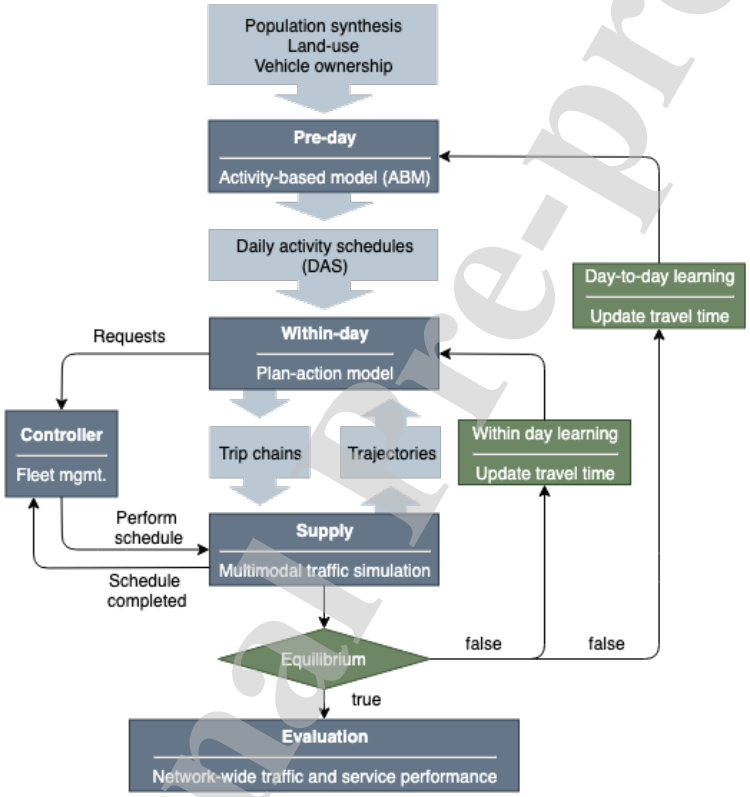

Figure 1: Simulation Framework

When idle, vehicles are directed to i) cruise within a specific area (i.e. high demand zone) or ii) drive to a parking location (i.e. the nearest available) until the controller finds a new request to assign to the vehicle.

In order to ensure equilibrium (or consistency) between demand and supply, after running the *Supply* simulation for a given scenario, we iteratively adjust the travel time tables (comprising of link travel times and public transit waiting times). The objective of the within-day learning process is to achieve equilibrium with regard to route choice decisions. Specifically, we compute the travel time in iteration i+1 (t_{i+1}) as a weighted sum of the current travel time from the supply simulation (t_S) and travel time in iteration i (t_i): $t_{i+1} = t_i * w + t_S * (1 - w)$, where w is a parameter. This process is repeated until the travel times in successive iterations (t_{i+1}, t_i) converge. Similarly, the day-to-day learning process enables the *Pre-day*

model system to adjust the individual activity schedules with updated travel times (including zone-to-zone travel-times, waiting times for public transit and waiting times for MOD and AMOD services). This process allows for the re-evaluation of accessibility, using agents' actual travel-times, experienced during the *Supply* simulation and arrive at a 'day-to-day' equilibrium.

3.2. Network Performance

As noted previously, the multimodal *Supply* simulation provides detailed information of individual agent and service vehicle trajectories. Travel trajectories contain information about the departure/arrival time at origin/destination, travel distance, and travel mode of each individual agent. Service vehicle trajectories contain information regarding schedule items performed by each service vehicle and their status in each time interval. These trajectories allow us to estimate network-wide traffic measures.

Network performance of each scenario is evaluated using suitable macroscopic variables, as detailed subsequently. Density is measured at the segment level (k_n for segment n) across the network and vehicle accumulation ($\mathcal{A}_V$, unit: veh; note that the subscript V denotes vehicles and P denotes passengers) is given by :

$$\mathcal{A}_V = \frac{\sum_n^{N_s} k_n \cdot l_n}{\sum_n^{N_s} l_n} \cdot L_N \tag{1}$$

Where, l_n is the length of segment n; L_N is the total network length. N_s represents the number of segments equipped with sensors and is a subset of the total number of segments N. While N_s would be useful from a practical implementation perspective, in this paper, data from all links are made available to us ($N_s = N$). The resulting accumulation may also be expressed as the sum of accumulations of each mode (at the vehicle level):

$$\mathcal{A}_V = \sum_{v \in V} \mathcal{A}_v \tag{2}$$

Where, $\mathcal{V}$ denotes the set of road-based modes. Also note that the spatial density variability (γ, unit: veh/km) is measured using the standard deviation of segment density (k_n) as in Eq. 6. Vehicle production ($\mathcal{P}_V$, unit: veh-km/hr) represents the total travel distance (VKT) driven by vehicles per unit time which can be quantified using the flow at each segment q_n:

$$\mathcal{P}_V = \frac{\sum_n^{N_s} q_n \cdot l_n}{\sum_n^{N_s} l_n} \cdot L_N \tag{3}$$

As noted previously, the travel trajectories capture detailed information of the mobility pattern of each individual vehicle/passenger including departure time, origin/destination, activity details (type and duration), travel (waiting) times, and average trip distances (TD_V, TD_P). Information is also available for respective trip completion rates (TC_V and TC_P, unit: trips/hr) that provide the number of completed trips per unit time. The production of passenger flow ($\mathcal{P}_P$) is thus estimated using the trip completion rate (TC_P) and average trip distance (TD_P) at the passenger level as,

$$\mathcal{P}_P = \sum_{p \in P} TC_p \cdot TD_p \tag{4}$$

Where, $\mathcal{P}$ denotes the set of all passenger modes. Equation 4 allows us to accurately measure production of passenger flow without the need to use average passenger occupancy as is typically done (Geroliminis et al. (2014); Ampountolas et al. (2017); Loder et al. (2017)). The number of travelers in the simulation (captured at each time interval over the entire network) represents the passenger accumulation ($\mathcal{A}_P$). Modes at the vehicle (V) and passenger level (P) are summarized in Table 3 in Section 5.1.

With this background, the MFD expresses the network production ($\mathcal{P}$) as a function of accumulation ($\mathcal{A}$) and congestion heterogeneity (γ) as in the literature (i.e. Knoop and Hoogendoorn (2013); Ramezani et al. (2015)),

$$\mathcal{P} = f(\mathcal{A}, \gamma) \tag{5}$$

The heterogeneity term γ typically refers to the spatial spread of density:

$$\gamma = \sqrt{\frac{\sum_n^N (k_n - \overline{k})^2}{N-1}} \tag{6}$$

MFD-based models have been extended to address congestion heterogeneity, as well as multimodality in various networks as described in Section 2.2. In this paper, we adapt the exponential form found to be applicable to multimodal traffic (Geroliminis et al. (2014)) as well as heterogeneous urban networks (Ramezani et al. (2015)). This approach formulates the *vMFD* and *pMFD*, corresponding to vehicles and passengers, as:

$$\mathcal{P}_V(A_V, \gamma) = a \cdot \mathcal{A}_V \cdot e^{b\mathcal{A}_V^3 + c\mathcal{A}_V^2 + d\mathcal{A}_V + r\gamma} \tag{7}$$

$$\mathcal{P}_P(\mathcal{A}_V, \gamma, \mathcal{A}_P) = a \cdot \mathcal{A}_V \cdot e^{b\mathcal{A}_V^3 + c\mathcal{A}_V^2 + d\mathcal{A}_V + r\gamma + \rho\mathcal{A}_P} \tag{8}$$

where a, b, c, d, r, ρ are model parameters.

4. Scenarios

The simulation scenarios in this study utilize a model of Singapore for the year 2030. The synthetic population of individuals and households (that are the inputs to the SimMobility Mid-term simulator shown in Figure 2) were generated by a Bayesian network approach (Sun and Erath (2015); details of the synthetic population can be found in Oh et al. (2020b)). The network (Figure 3) consists of 1,169 traffic analysis zones, 6,375 nodes, 15,128 links, and 30,864 segments. The total network length (L_N) is approximately 3,175km, and includes 730 bus lines serving 4,813 bus stops, and 26 MRT (rail) lines serving 186 stations.

Travel and activity demand is estimated by the *Pre-day* ABM system using the synthetic population for year 2030 (for more details on estimation and calibration of the ABM system refer to Oh et al. (2020b)) and also draws on data from a smartphone-based state preferences (SP) survey on AMOD (Seshadri et al. (2019)). Three scenarios are considered with regard to the price or fare of the AMOD services:

- AMOD single-ride price: 75%, 100% and 125% of taxis
- AMOD shared-ride price: 75% of single-ride

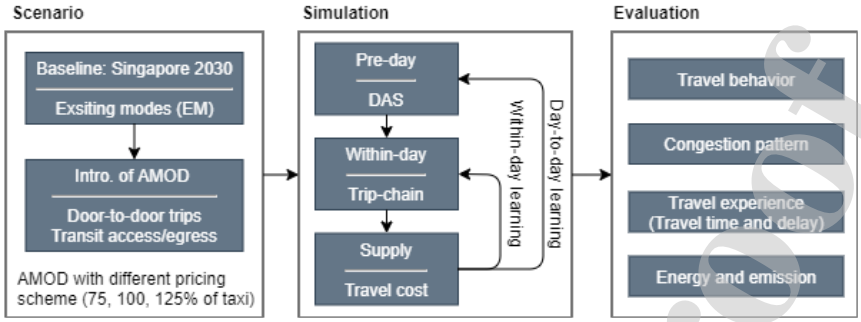

Figure 2: Evaluation Framework

Figure 3: Network Topology in Singapore

Note that the taxi fare (f_{taxi}, unit: SGD) is determined as:

$$f_{taxi} = f_{base} + f_{km} * td_0 + f_{min} * tt_0 \tag{9}$$

In which, $f_{base} = 3.2$, $f_{km} = 0.55(< 10km), 0.63(> 10km)$ per km, $f_{min} = 0.29$ per min, and tt_0 and td_0 represent the proxy of travel time and distance from a *skim* matrix of travel cost estimates between zones. The key reason for using the taxis as a benchmark is that existing literature on potential pricing of AMOD services has typically pegged it against taxis, and this provided some rationale for the choice of levels (Bösch et al. (2018), Spieser et al. (2014)). More importantly, the per-distance cost of traditional taxis versus MOD in Singapore are in fact very similar (0.55 S$/km versus 0.5 S$/km), and further, the taxi tariff structure in Singapore also includes surcharges for the peak period, similar to the surge pricing in the case of on-demand services.

Thus, we simulate four scenarios of interest that differ in modal availability and AMOD pricing: Baseline, and three AMOD scenarios with different pricing schemes (75%, 100% and 125% of taxis). In the baseline, travel modes available to agents are the existing modes (EM),

which include private car, car-pooling (with 2 or 3 people per household), private bus, walking, taxi, MOD (Uber-like ride-sourcing services), public transit (bus, rail) with access/egress by walk. In the AMOD scenarios, in addition to the existing modes, the AMOD service is made available to travelers. AMOD services include door-to-door services with single/shared rides and first/last-mile connectivity to public transit (e.g. rail station).

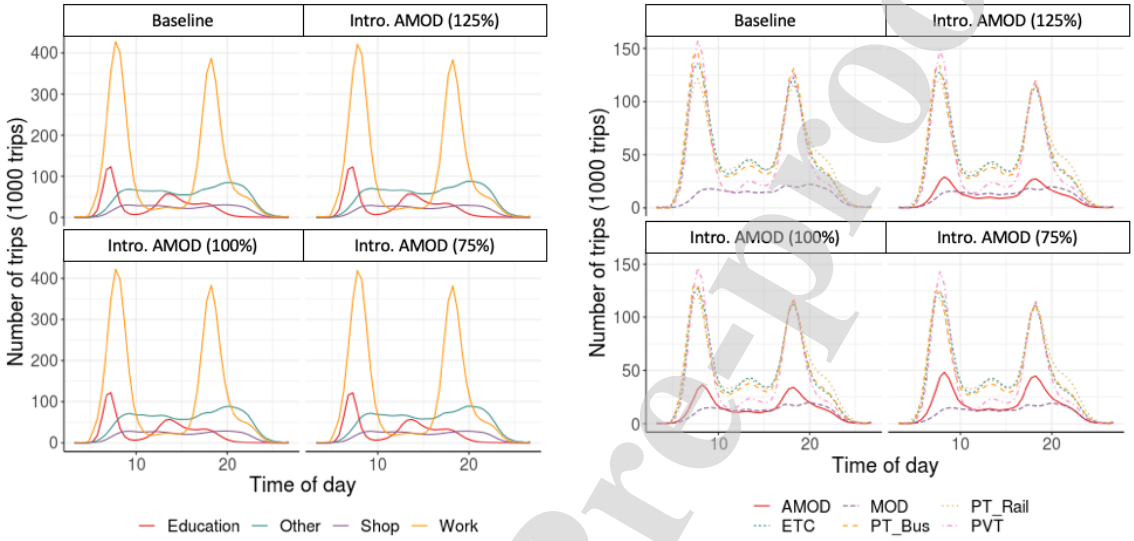

(a) By Activity Type (b) By Mode

Figure 4: Travel Demand Pattern over Time-of-day

Figure 4 shows the distribution of demand for the different pricing scenarios by mode and activity types, each of which shows a different temporal pattern (Figure 4a). The *Work* trips comprise the largest portion of trips particularly during the peak periods. *Education* trips show similar patterns with *Work* in the morning, however, as expected, many trips occur before the PM peak period (around 2–3PM). Trips for *Shopping* and *Other* activities (such as leisure, recreation) are observed throughout the day. A large number of additional trips for *Other* activities occur during and after PM peak.

Table 1 lists the mode shares for each scenario (temporal distribution in Figure 4b). The total number of passenger trips for 24 hours is 8,991,057 trips (baseline), 8,995,544 trips (75% pricing), 8,992,168 trips (100% pricing), 8,994,926 trips (125% pricing). These passenger trips (around 9 million) for all scenarios are simulated along with background traffic of freight vehicles (665,929 trips) estimated by the SimMobility Freight model (Sakai et al. (2019)). As expected, the introduction of AMOD leads to a reduction in the share of existing modes. Particularly, the share of public transit (PT), including Bus and Rail, reduces by 2.39–3.86%, while reductions in the number of private vehicle trips (PVT) are smaller in magnitude (1–2%). Thus, a large portion of AMOD demand (door-to-door service with AMOD single/shared) includes shifts from PT with walk access (more than 55%), while the shift rates from other modes are relatively low (around 4%, 14%, 5% of AMOD demand are from private car, taxi, and MOD trips, respectively). Overall, the shares of AMOD range from 5.77–8.87% across the three pricing scenarios, while the shifts from original share of PT with walk access to PT access by AMOD are significantly smaller.

Table 1: Mode Share

Modes		Baseline	Intro. of AMOD		
			75%	100%	125%
PVT	Car/Carpool	18.75%	17.33%	17.7%	17.93%
	Taxi	2.16%	1.6%	1.69%	1.75%
PT	Bus	24.33%	21.49%	22.14%	22.57%
	Rail(Walk)[a]	23.81 %	20.54 %	21.21%	21.67%
	Rail(MOD)[a]	0.36%	0.3%	0.32 %	0.32%
	Rail(AMOD)[a]	0	2.31%	1.88%	1.55%
MOD	Single/Shared	6.41%	5.38%	5.51%	5.64%
AMOD	Single/Shared	0	8.87%	7.01%	5.77%
Other		24.16%	22.18%	22.54%	22.79%

[a] Access/egress to/from rail station by Walk, MOD, and AMOD respectively.

The large difference between the share of MOD and AMOD can be explained with the differences in perception of users towards AMOD relative to MOD, based on data from the state preferences survey in Seshadri et al. (2019) which suggest the users tend to prefer the AMOD services (with all other factors being the same) with an inclination towards new services and technologies and the guarantee of AV safety.

On the supply, the public transit vehicles (buses and trains) operate in accordance with fixed schedules as described in Section 3.1. Regarding the on-demand services, the fleet sizes for the three AMOD pricing scenarios (75%, 100% and 125% respectively) are fixed at 43,000, 33,000, and 27,000 vehicles comprising 4- and 6-seaters (see Oh et al. (2020b) for more details). Note that this fleet size is derived by finding an *optimal* size, which yields sufficient fleet utilization (minimizing the number of idle vehicles during peak period), reasonable passenger waiting times (less than 6 min) and service satisfaction rates (serving all incoming requests). The required MOD fleet size ranges from 20,000–22,000 for each scenario. The on-demand service vehicles are operated using the assignment and rebalancing algorithms of the *SMS controller*. The assignment parameters (wt_{min}, tt_{ad}) are set to 10 min, and vehicles are set to cruise during the rebalancing interval (1 min) and directed to the nearest available parking if there is no additional service assignment.

Table 2 summarizes the simulation configurations and scenario factors described in this section. Each scenario was simulated via several iterations of the *within-day* and *day-to-day learning* process to ensure the consistency between demand and supply.

5. Results and Analysis

5.1. MFD: Analysis, Modeling, and Estimation

The *Supply* module simulates multimodal network performance (travel demand from the pre-day and within-day models) and specifically, all modes listed in Table 3. For our analysis, the modes have been classified into two categories, based on whether they contribute to vehicle (*vMFD*) and passenger flow (*pMFD*) respectively. First, the private vehicle trips

Table 2: Experimental Settings

Factor		Scenarios			
		Baseline	Intro. AMOD		
			75%	100%	125%
Simulation config.	Simulation model	SimMobility Mid-term			
	Simulation period	24 hours			
	Scope of simulation	Singapore network with 6.5M agents			
Scenario factor	Modal availability	Existing modes (EM)	EM + AMOD		
	Num. of trips[a]	9,656,986	9,661,473	9,658,097	9,660,855
	Fleet size[b]	-	43,000	33,000	27,000
	Fleet composition	-	4- and 6-seaters		
	Fleet assignment	$wt_{min}, tt_{ad} = 10min$, s.t. availability($C_v$)			
	Fleet rebalancing	Rebalancing every 1min interval			

[a] This total number of trips include 665,929 freight trips across all scenarios.
[b] Fleet size taken from Oh et al. (2020b).

(PVT) contribute to both passenger and vehicle traffic on the network. In the case of on-demand services, MOD and $AMOD$ contribute to both categories when the service vehicle drives with passenger(s). In contrast, MOD_{OP} and $AMOD_{OP}$ represent operational movements, including empty trips to pick up the passenger, cruising for parking or moving to a parking location, and hence, contribute to only vehicle traffic. Public transit passenger trips are captured by the modes Bus (or $Rail$) at the passenger level, while Bus_{OP} represents the bus vehicle movement with fixed routes and schedules. Also note that all trains (labeled as $Rail_{OP}$) are operated on the rail network and do not directly affect road network traffic. Other modes (labeled as $Other$) were also considered, such as $walking$, for passenger flow estimation. As noted in Section 4, the freight commodity flow is considered through background freight traffic and accounted for in the vehicle flow estimation.

Figure 5 presents the temporal distribution of network-wide production of vehicle ($\mathcal{P}_V$) and passenger flow ($\mathcal{P}_P$). At the vehicle level (Figure 5a), one can notice that traffic flow increases significantly from the baseline scenario with the introduction of AMOD, especially during the peak periods. Moreover, in the lower pricing scenarios, which require a larger fleet size to accommodate the higher AMOD demand (Table 2), we observe increased traffic flows than in the higher pricing case (125% scenario). In contrast, unlike vehicle production, passenger production curves (Figure 5b) do not change significantly across scenarios, indicating that the temporal distribution of passenger flows is not significantly affected by the increased traffic flows on the network.

Figure 6a plots the $vMFD$, which relates the production of vehicle traffic ($\mathcal{P}_V$) with vehicle accumulation ($\mathcal{A}_V$) and spatial variability of density (γ). The time-of-day is also marked on each point of production/accumulation in the figure. Two distinct patterns are visually identifiable, showing the loading and unloading of traffic congestion before and after AM and PM peak periods. Comparing the scenarios, the maximum accumulation of vehicles during the peak increases by 8.7–14.5% in the AMOD scenarios (150,778, 150,274, 143,155

Table 3: Travel Modes

Category	Mode	Vehicle flow (*vMFD*)	Passenger flow (*pMFD*)
PVT	$Car/Carpool$	✓	✓
	$Taxi$	✓	✓
MOD	MOD	✓	✓
	MOD_{OP}[a]	✓	-
AMOD	$AMOD$	✓	✓
	$AMOD_{OP}$[a]	✓	-
PT	Bus	-	✓
	Bus_{OP}[b]	✓	-
	$Rail$	-	✓
	$Rail_{OP}$[c]	-	-
Other		-	✓
Freight		✓	-

[a] $MOD_{OP}/AMOD_{OP}$ represents empty trips made by MOD and AMOD service vehicles for operational purposes (such as driving to passenger, parking, cruising).
[b] Travel details on Bus_{OP} is collected from the bus trajectory with the predefined lines and frequency.
[c] Trains are operated in an underground rail network ($Rail_{OP}$) and excluded from both levels.

vehicles for the 75%, 100%, and 125% scenario respectively) from that of baseline (131,689 vehicles). In the case of vehicle production, maximum production increases by about 5.6–8.8% from the baseline to AMOD scenarios: 4,186,462 veh-km/hr (Baseline), 4,553,106 veh-km/hr (75% pricing), 4,474,012 veh-km/hr (100% pricing), and 4,419,385 veh-km/hr (125% pricing). The heterogeneity of network congestion also increases in the AMOD scenarios: the maximum spatial variability of density (γ) increases from 88 (veh/km) in the baseline to 97–102 (veh/km) in the AMOD scenarios at around 8AM (morning peak period). This increase in heterogeneity leads to the appearance of clockwise hysteresis loops in the *vMFD*, which demonstrate the delay in the recovery of production from the congested state. We quantify the magnitude of hysteresis (Geroliminis and Sun (2011)) by the gap between the production values when loading ($\mathcal{P}_V^l$) and unloading ($\mathcal{P}_V^u$) at a given accumulation level as:

$$h(\mathcal{A}_V) = \Delta\mathcal{P}(\mathcal{A}_V) = \mathcal{P}_v^l(\mathcal{A}_V) - \mathcal{P}_v^u(\mathcal{A}_V) \tag{10}$$

Note that in computing the hysteresis, we have used a smoothing spline estimate (Kimeldorf and Wahba (1970)) to interpolate the production values where required. Figure 7 compares the magnitude of hysteresis between the baseline and the 125% pricing scenario. In the baseline, the maximum value is 549,065 and 386,942 (veh-km/hr) during the AM and PM peak period respectively. In the AMOD scenario, $h(A_V)$ increases to 649,216–653,581 and 547,930–591,355 (veh-km/hr) for the two peak periods. The total hysteresis during AM and PM peak period ($\mathcal{H} = \int_{t=1}^{T} h(\mathcal{A}_V)dt$) increases by around 24.49–28.56% when introducing the AMOD service.

According to Eq.7, the shape of the MFD is determined by the two variables ($\mathcal{A}_V$, γ) and

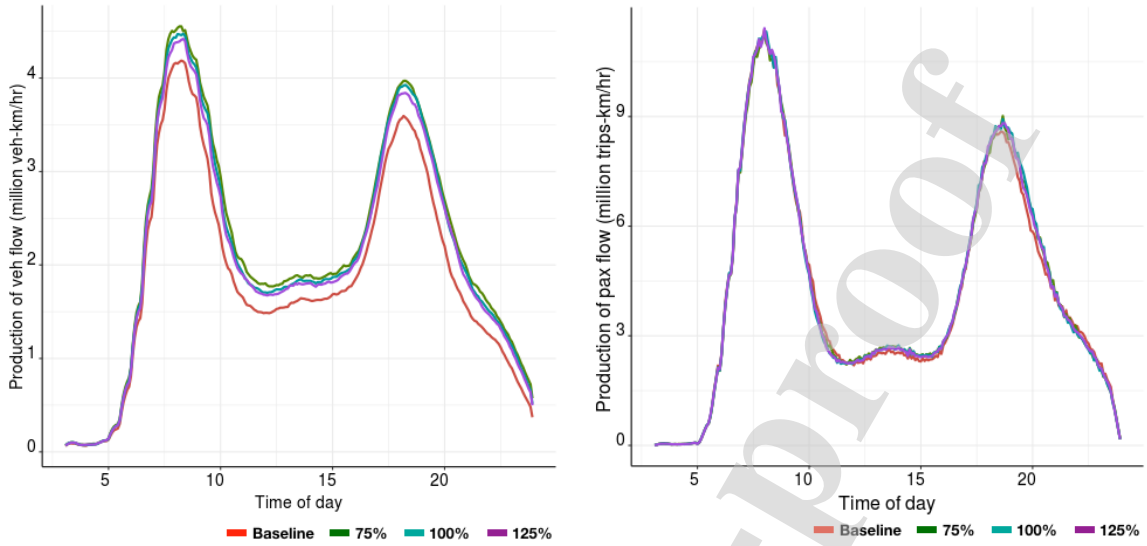

(a) Simulated P_V (b) Simulated P_P

Figure 5: Distribution of Network Production over Time-of-day

model parameters (a, b, c, d, r). We estimate the parameters using a nonlinear least squares method (Kass (1990)) to fit the simulated data ($\mathcal{P}_V^{'}$) with constraints on production $\mathcal{P}_v(\geqslant 0)$, accumulation $\mathcal{A}_V$ $(0 \leqslant \mathcal{A}_v \leqslant max(\mathcal{A}_V^{'}))$ and space-mean speed $\mathcal{S}(\forall v \in \mathcal{V} : \partial \mathcal{S}_V / \partial \mathcal{A}_v \leq 0)$, where $v \in V$ (set of road-based modes).

$$\min_{a,b,c,d,r} \mathbf{Z} = \|\mathcal{P}_V - \mathcal{P}_V^{'}\|^2 \tag{11}$$

Table 4 lists the estimated parameters, which were all found to be statistically significant. The predicted vehicle production curve (based on the fitted model) for each scenario is shown by the red line in Figure 6b, which illustrates the evolution of network dynamics by time-of-day and captures the hysteresis loops during the on- and off-set of congestion. The discrepancy between the simulated and predicted production is measured using the normalized root mean square error (RMSN) in Eq. 12, and ranges between 0.034–0.036% over the scenarios.

$$RMSN = \frac{\sqrt{T \sum_{t=1}^{T} [\mathcal{P}_V(t) - \mathcal{P}_V^{'}(t)]^2}}{\sum_{t=1}^{T} \mathcal{P}_V^{'}(t)} \tag{12}$$

In case of the *pMFD*, Figure 8a shows the production of passenger flow with respect to the aggregate number of vehicles on the network and the spatial variability of density. The shape of the *pMFD* is different from that observed in the case of the *vMFD*. It shows (i) a larger gap between two production curves of loading and unloading during the AM peak (resulting in large clockwise hysteresis loops), and (ii) small counter-clockwise hysteresis loop during the PM peak. These two points can be attributed to the nature of passenger trip distances as elaborated below:

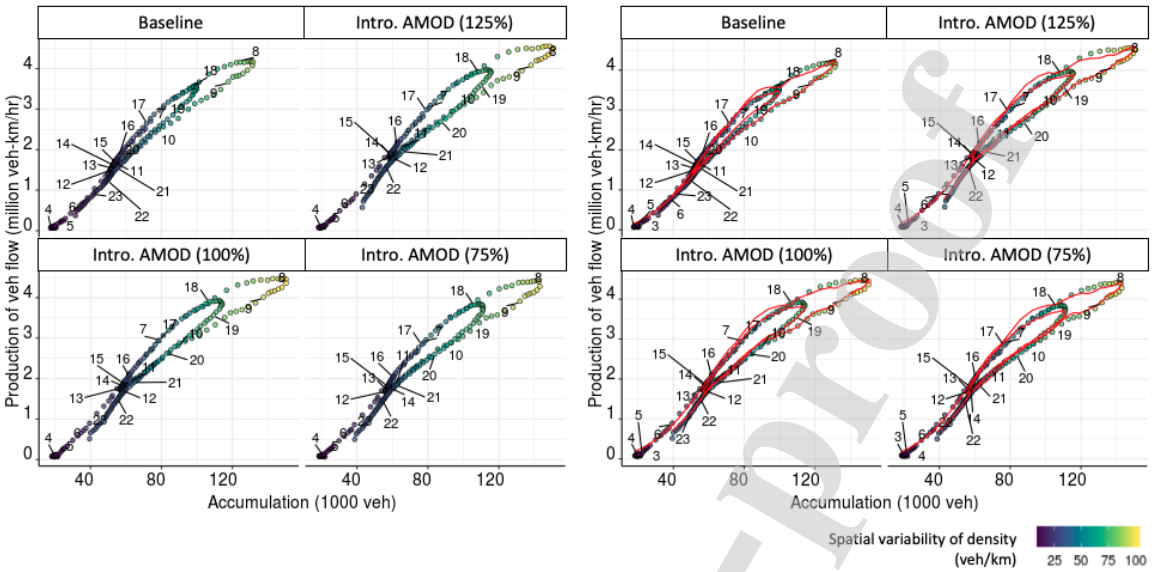

(a) Simulated $\mathcal{P}_\mathcal{V}$ (b) Predicted $\mathcal{P}_\mathcal{V}$ (Red)

Figure 6: *vMFD*: $\mathcal{P}_V = f(\mathcal{A}_V, \gamma)$

(i) Difference in the average trip distances at the vehicle and passenger level ($TD_V > TD_P$). The average trip distance of vehicle (TD_V) reduces from around 12.5km (while loading) to 10–11km (while unloading after 8:30AM). In case of TD_P, it decreases more significantly from around 9km (while loading) to 6.5km (while unloading). Since the production is determined by both trip completion rate and trip distance, the larger decrease in TD_P results in a higher trip completion rate, as well as a larger gap of $\mathcal{P}_p$ between the loading and unloading in case of the *pMFD*.

(ii) Longer trip distances while unloading during the PM peak period. The passenger trip distance (TD_P) appears to be longer than 8km after 7PM, during the unloading, while being shorter (7–8km) for those trips completed before 7PM, during the loading. This contributes to higher production during unloading and results a counter-clockwise hysteresis loop. Additional clues can be found in the temporal demand pattern by activity types (see Section 4): more trips (e.g. *Other* activity in Figure 4a) are generated and contribute to higher production in the offset of congestion during the PM peak period.

In a similar manner as the $vMFD$, we estimate the model described in Eq.8 and the estimated parameters are summarized in Table 4, all of which were found to be statistically significant. The discrepancy between simulated and predicted passenger productions (quantified by the RMSN) are found to range between 0.074–0.079 % across the scenarios. Also, as shown in Figure 5b and Figure 8a, the maximum and overall temporal patterns of passenger production ($\mathcal{P}_P$) remain similar across the scenarios, in contrast with the the distinct impacts on $\mathcal{P}_V$ in the $vMFD$ observed with the introduction of AMOD. This may be ascribed to a range of factors, one of which is the cannibalization of transit by AMOD (explained in Section 4). Even though the road network congestion is more severe in the AMOD scenarios

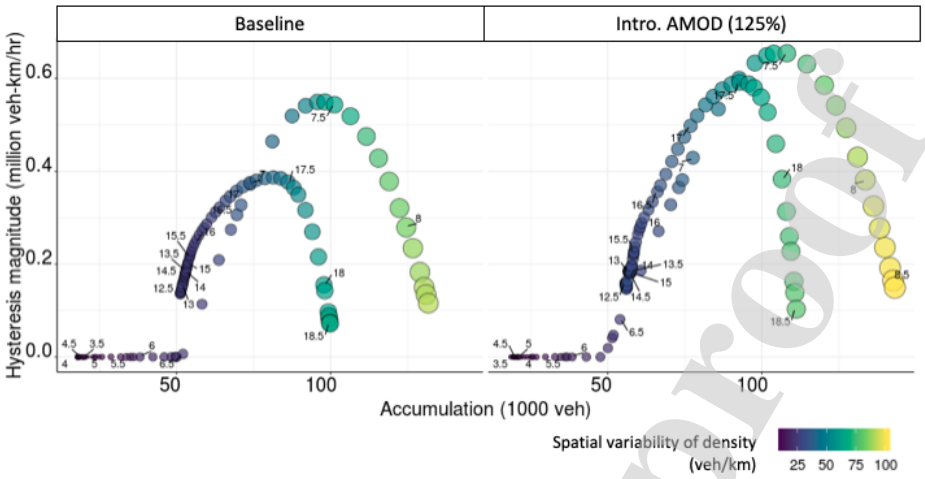

Figure 7: Magnitude of Hysteresis ($h(\mathcal{A}_V)$)

(as verified in Section 5.2.2), the effects of network congestion on the production of passenger flow may be minimal as a significant share of AMOD ('faster' modes in general but which are affected by the additional network congestion) includes shifts from transit ('slower' modes in general but which are unaffected by network congestion).

Table 4: Estimation Result for *MFD*

Model		**Parameters**					
		a	b	c	d	ρ	r
vMFD	Baseline	0.284	$7.50 \cdot 10^{-5}$	$-6.28 \cdot 10^{-10}$	$1.954 \cdot 10^{-15}$	-	−0.01346
	75%	0.328	$6.65 \cdot 10^{-5}$	$-4.79 \cdot 10^{-10}$	$1.286 \cdot 10^{-15}$	-	−0.01462
	100%	0.366	$6.26 \cdot 10^{-5}$	$-4.38 \cdot 10^{-10}$	$1.151 \cdot 10^{-15}$	-	−0.01465
	125%	0.298	$7.10 \cdot 10^{-5}$	$-5.42 \cdot 10^{-10}$	$1.537 \cdot 10^{-15}$	-	−0.01452
pMFD	Baseline	0.608	$6.42 \cdot 10^{-5}$	$-8.99 \cdot 10^{-10}$	$2.94 \cdot 10^{-15}$	$5.22 \cdot 10^{-6}$	0.00634
	75%	0.734	$5.07 \cdot 10^{-5}$	$-5.73 \cdot 10^{-10}$	$1.654 \cdot 10^{-15}$	$5.39 \cdot 10^{-6}$	−0.00705
	100%	0.662	$5.48 \cdot 10^{-5}$	$-6.12 \cdot 10^{-10}$	$1.794 \cdot 10^{-15}$	$4.84 \cdot 10^{-6}$	−0.00534
	125%	0.622	$5.70 \cdot 10^{-5}$	$-6.85 \cdot 10^{-10}$	$2.04 \cdot 10^{-15}$	$5.19 \cdot 10^{-6}$	−0.00207

Table 5: Primary (Well-to-wheels) Energy Consumption (unit: kWh)

	Fuel						Electricity		
Scenarios	$v = PVT$	Bus_{OP}	MOD	MOD_{OP}	$Freight$	Total	$AMOD$	$AMOD_{OP}$	Total
Baseline	10,186,083	505,332	2,901,130	1,337,413	3,798,208	18,728,167	0	0	0
75%	9,398,493	503,049	2,254,457	1,003,054	3,665,271	16,824,324	4,107,287	2,354,117	6,461,405
100%	9,596,024	503,917	2,394,551	1,098,965	3,663,389	17,256,844	3,344,555	1,905,370	5,249,925
125%	9,693,896	504,227	2,477,469	1,154,828	3,661,884	17,492,304	2,815,517	1,593,608	4,409,125

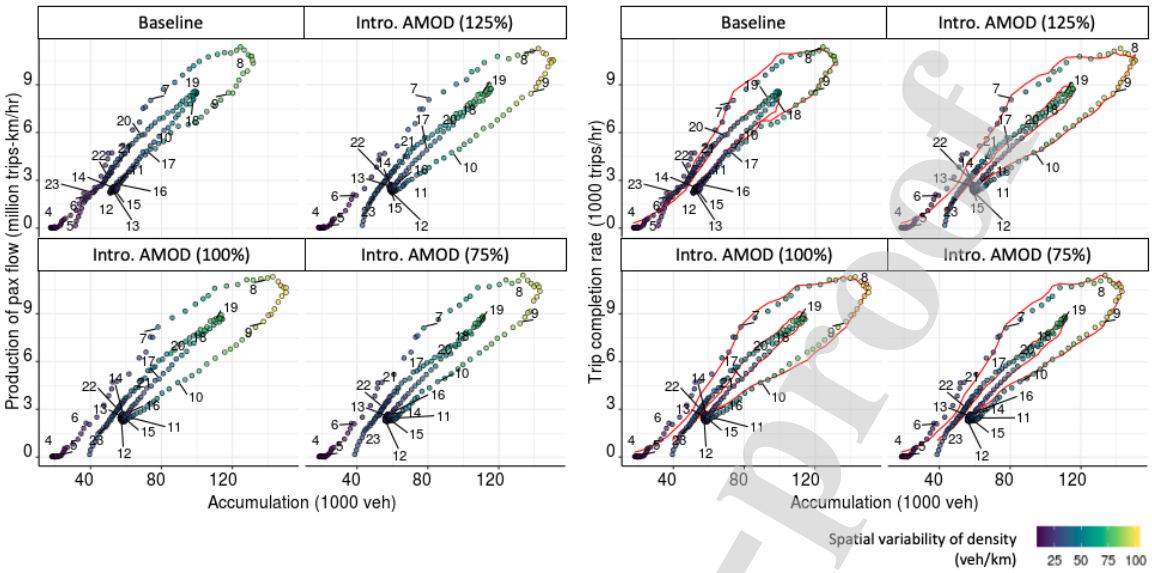

(a) Simulated $\mathcal{P}_{\mathcal{P}}$ (b) Predicted $\mathcal{P}_{\mathcal{P}}$ (Red)

Figure 8: *pMFD*: $\mathcal{P}_P = f(\mathcal{A}_V, \gamma)$

Table 6: Vehicle Emission: NO_x and PM (unit: kg)

Scenarios	$v = PVT$		Bus_{OP}		MOD		MOD_{OP}		$Freight$		Total	
	NO_x	PM	NO_x	PM	NO_x	PM	NO_x	PM	NO_x	PM	NO_x	PM
Baseline	1080.6	72.3	963.4	17.9	272.9	20.6	125.9	9.5	2856.8	63.1	5299.7	183.4
75%	993.1	66.7	954.1	17.8	209.8	16.0	93.3	7.1	2745.9	60.6	4996.1	168.3
100%	1015.4	68.1	956.2	17.9	223.5	17.0	102.6	7.8	2746.5	60.7	5044.2	171.4
125%	1025.7	68.8	958.2	17.9	231.6	17.6	108.1	8.2	2744.5	60.6	5068.1	173.1

5.2. Impacts on Energy, Emissions and Congestion

5.2.1. Energy and Emissions

In this section, we examine the impacts of AMOD on energy and emissions at the network level. We assume that the AMOD fleet is fully composed of battery electric vehicles (BEV) and the other vehicle categories are composed of gasoline/diesel-fueled vehicles (Euro 6 standard for passenger vehicles, bus, and freight trucks). Table 5 and Table 6 summarize the emissions and energy consumption for each travel mode (v) based on the total vehicle-km traveled (VKT). Note that this VKT is equivalent to the total $\mathcal{P}_V$ for 24h, which is 31.78, 37.65, 36,65, and 35.51 million-km for the baseline, 75%, 100%, and 125% scenarios respectively. As noted previously, we observe a significant increase in VKT ranging from 11.8-18.5% for the AMOD scenarios, compared to the baseline.

Energy consumption of the AMOD fleets is measured using an average energy consumption rate (ECR). According to real-world estimation data (Fetene, 2014), the ECR decreases with vehicle travel distance as follows: 233Wh/km, 183Wh/km, 166Wh/km for short ($TD_v \leq 2km$), medium ($2km \leq TD_v \leq 10km$), and long distances ($TD_v \geq 10km$). The energy consumption is computed by multiplying the production factor (2.99, US average

energy-to-fuel ratio), which incorporates well-to-wheels effects while taking into account the transmission and distribution losses of BEVs. Accordingly, the total energy consumption is 6.46GWh, 5,25GWh, 4,41GWh for the 75%, 100%, 125% scenarios respectively. As anticipated, the increase in VKT, in lower pricing scenarios, results in larger energy consumption for both service and operational purposes. Note that a significant portion of energy consumption is caused by the operating trips (empty trips for passenger pick-up, cruising, parking) taking around 36% of total energy consumption across AMOD scenarios. Further, for the existing road-based modes (non-electric vehicles), we compute energy consumption using the miles per gallon gasoline equivalent (MPGe) of each vehicle type. By assuming the future MPGe as 47(5.0L/100km) and 52(4.5L/100km) for gasoline and diesel-powered vehicles respectively (Ec.europa.eu), total consumption (by PVT, Bus_{OP}, MOD, MOD_{OP}, $Freight$) is determined to be 18.73GWh, 16.82GWh, 17.26GWh, and 17.49GWh for the four scenarios respectively. Note that 1 MPGe is equivalent to 0.04775km/kWh (EPA (2011)) and the corresponding average energy-to-fuel ratios are 1.17 and 1.05 for gasoline and diesel respectively. Thus, total energy consumption by all vehicles increases with the introduction of AMOD by 24.33%, 20.18%, and 16.94% for the 75%, 100%, and 125% scenarios respectively.

In the case of vehicle emissions, we consider the production of NO_x and PM (exhaust particulate matter) by passenger cars as well as buses and trucks on the network. According to the emission testing (Euro-6 standard) results in Ligterink (2017), the unit emissions for NO_x and PM are estimated dependent on vehicle types (passenger cars, buses, trucks) and congestion as: 0.043–0.063g/km (NO_x), 0.0037g/km (PM) for passenger car (petrol), 0.69–1.11g/km (NO_x), 0.015g/km (PM) for buses, 0.28–0.44g/km (NO_x), 0.0061–0.010g/km (PM) for trucks. Total emissions reduce with the introduction of AMOD from 5,299.7kg (NO_x) and 183.4kg (PM) in baseline to 4,996–5,068kg (NO_x) and 168–173kg (PM) in the AMOD scenarios. In summary, the introduction of AMOD may bring about significant emission reductions (4.3–5.7% in NO_x and 5.6–8.2% in PM), while resulting in more energy consumption (up to 24.33% from the baseline scenario).

5.2.2. Congestion and Delay

The increase in network traffic contributes to congestion and travel delays. In order to further quantify network congestion, we examine the distance weighted trip speed index (TSI_V) using the individual vehicle's trip speed (TS_v) and the travel distance from origin to destination (TD_v):

$$TSI_V = \frac{\sum_v \left(TD_v * (TS_v/TS_v^0)\right)}{\sum_v TD_v} \tag{13}$$

where, TS_v^0 is the free-flow speed between origin and destination of individual v. Clearly, as seen in Figure 9a, the trip speed index decreases from 1 in the off-peak period (free-flow) to values of around 0.65 and 0.8 in the AM and PM peak periods respectively. Furthermore, the TSI_V for AMOD scenarios decreases significantly during the peak periods by 8–11.9% (AM) and 7.8–9.7% (PM) from the baseline.

The increase in VKT and decrease in network speed, as expected, affect travel experience. We quantify this effect using a measure of delay in travel-time (IVD_v) at the individual level (v):

$$IVD_v = IVTT_v - IVTT_v^0 \tag{14}$$

where, $IVTT_v$ is the in-vehicle travel-time of individual vehicles; $IVTT_v^0$ is the free-flow travel time. The distributions of $IVTT_v$ and IVD_v are shown in Figure 9b. Compared to the baseline (5.2 and 3.7min of IVD_v for AM and PM peak period), IVD_v increase ranges from 7.8–15%, 20–23% for AM and PM peak periods across the AMOD scenarios.

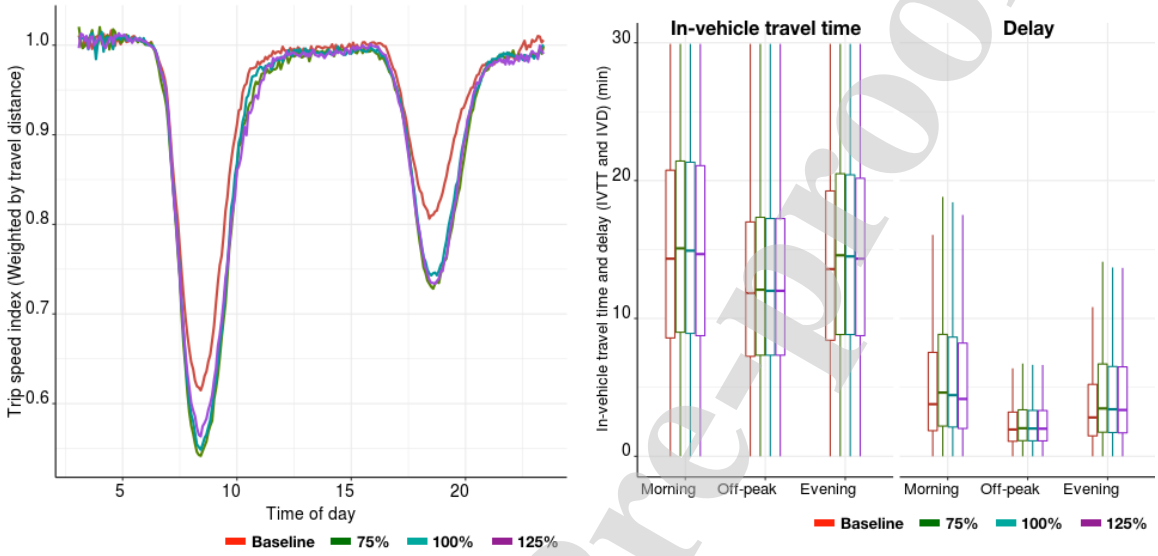

(a) Trip Speed Index (TSI_V)

(b) $IVTT_v$ and IVD_v

Figure 9: Congestion Effects

Finally, we measure the changes of travel times of individual travelers p with mode v. The journey time ($JT_{p,v}$) is the sum of two components:

$$JT_{p,v} = WT_{p,v} + IVTT_{p,v} \tag{15}$$

where, $WT_{p,v}(= wt_{p,v} + aet_{p,v})$ includes the individual waiting time ($wt_{p,v}$) for services of MOD, AMOD, PT, and the access/egress time ($aet_{p,v}$) by walk to/from bus stops and MRT(rail) stations for transit service; $IVTT_{p,v}$ is the in-vehicle travel-time of individual passengers with a chosen mode v (incl. EM (PVT, PT, MOD) and AMOD) for each journey.

As noted in Section 4, the introduction of AMOD may cause modal shifts of PT demand. Passengers are estimated to experience, on average, around 38.5 and 43.9 min of $JT_{p,PT}$ with 8.7 to 10.3 min of $WT_{p,PT}$ and 35.2 and 28.2 min of $IVTT_{p,PT}$ with public bus and rail service respectively. Figure 10 shows the changes in the average of journey time of AMOD users shifted from baseline: $WT_{p,EM}$ and $IVTT_{p,EM}$ in the baseline and $WT_{p,AMOD}$ and $IVTT_{p,AMOD}$ in AMOD scenarios. It shows a significant reduction of $JT_{p,v}$ of 'transit' users in baseline by 48–55% (single) and 37–45% (shared) with less waiting and travel time in AMOD scenarios. Note that the waiting times of AMOD are around 4.4 min (off-peak) and range from 5–6 min (during peak periods) on average (ranging between 1–3 min of delay). This waiting time ($WT_{p,AMOD}$) incurs additional travel times for 'PVT' passengers (in baseline) resulting in an increase in $JT_{p,AMOD}$ by 41–44% and 64–75% with AMOD single/shared.

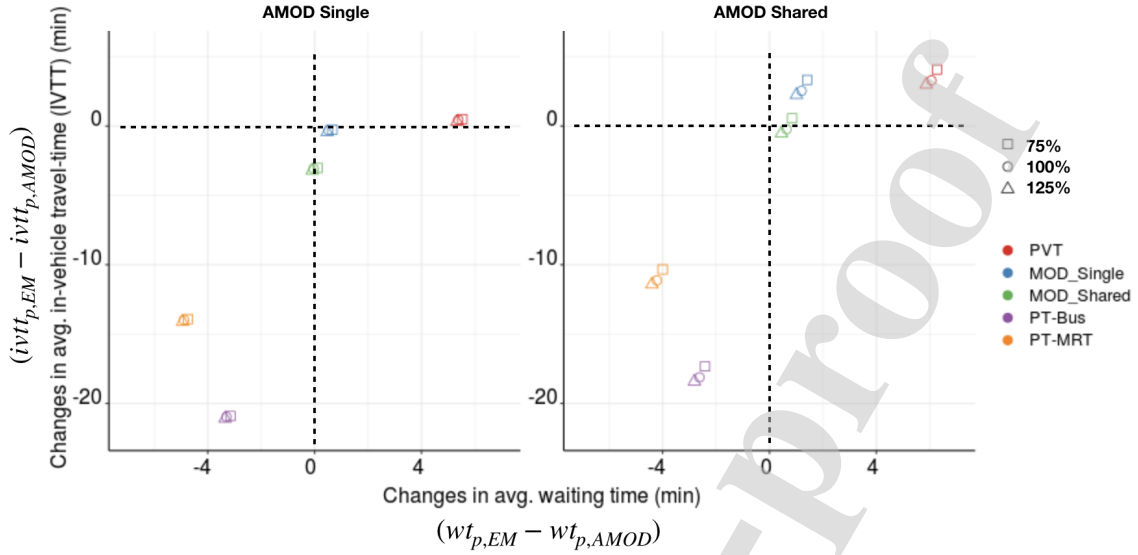

Figure 10: Changes in Journey Time of AMOD User

6. Conclusion

This paper evaluates the network impacts of AMOD on network traffic, congestion, energy, and vehicle emissions by utilizing agent-based simulation. The simulation framework models activity-based travel demand, supply (including fleet operations and multimodal network performance) and their interactions. Scenario simulations of the entire urban network of Singapore yield several insights into the impacts of AMOD: Introduction of AMOD services may induce additional vehicle traffic resulting in more congestion relative to the baseline scenario. The network congestion in AMOD scenarios is due in part to the demand patterns (i.e. cannibalization of transit shares) as well as dead-heading and empty trips for operational purposes. The vehicle accumulation and production increases by 8.7–14.5% and 5.6–8.8% respectively, and the total magnitude of hysteresis loops increases by more than 24% with the introduction of the AMOD service. Despite the increase in network congestion, the passenger production is not significantly impacted. The estimated models of *vMFD* and *pMFD* predict the production at the vehicle and passenger level and their dynamics accurately. In addition, the impacts of AMOD in terms of energy and emissions is quantified. The introduction of AMOD leads to increased energy consumption (by 16.94–24.33% from baseline), although vehicle emissions in terms of NO_x and PM are reduced (by 4.3–5.7% and 5.6–8.2%, respectively). The travel delay has been increased up to 23% in the case of the AMOD scenario with an increase of VKT, while the journey time of the travelers who shifted from transit to AMOD can be significantly improved.

Based on the simulation and modeling framework, several avenues for future research remain, including the testing of (existing/emerging) MFD-based and other traffic management measures and policies (i.e. vehicle quota systems, route guidance systems, perimeter control, congestion pricing in multimodal urban networks) for maximizing social welfare at both the local and urban scale. The proposed framework can also be applied to evaluate the effect of long-term impacts of AMOD on land-use as well as car-ownership, which are interesting

areas for future research.

Acknowledgements

This research is supported in part by the Singapore Ministry of National Development and the National Research Foundation, Prime Minister's Office under the Land and Liveability National Innovation Challenge (L2 NIC) Research Programme (L2 NIC Award No L2NICTDF1-2016-4). Any opinions, findings, and conclusions or recommendations expressed in this material are those of the author(s) and do not reflect the views of the Singapore Ministry of National Development and National Research Foundation, Prime Minister's Office, Singapore. Also, this research was supported by Basic Science Research Program through the National Research Foundation of Korea (NRF) funded by the Ministry of Education (NRF-2019R1A6A3A12031439).

References

Adnan, M., Pereira, F.C., Azevedo, C.M.L., Basak, K., Lovric, M., Raveau, S., Zhu, Y., Ferreira, J., Zegras, C., Ben-Akiva, M., 2016. Simmobility: A multi-scale integrated agent-based simulation platform, in: 95th Annual Meeting of the Transportation Research Board.

Ahn, S., Coifman, B., Gayah, V., Hadi, M., Hamdar, S., Leclercq, L., Mahmassani, H., Menendez, M., Skabardonis, A., van Lint, H., 2019. Traffic flow theory and characteristics. Centennial Papers .

Alonso-Mora, J., Samaranayake, S., Wallar, A., Frazzoli, E., Rus, D., 2017. On-demand high-capacity ride-sharing via dynamic trip-vehicle assignment. Proceedings of the National Academy of Sciences 114, 462–467.

Ambühl, L., Loder, A., Menendez, M., Axhausen, K.W., 2017. Empirical macroscopic fundamental diagrams: New insights from loop detector and floating car data, in: TRB 96th Annual Meeting Compendium of Papers, Transportation Research Board. pp. 17–03331.

Ampountolas, K., Zheng, N., Geroliminis, N., 2017. Macroscopic modelling and robust control of bi-modal multi-region urban road networks. Transportation Research Part B: Methodological 104, 616–637.

Azevedo, C.L., Marczuk, K., Raveau, S., Soh, H., Adnan, M., Basak, K., Loganathan, H., Deshmunkh, N., Lee, D.H., Frazzoli, E., et al., 2016. Microsimulation of demand and supply of autonomous mobility on demand. Transportation Research Record 2564, 21–30.

Basu, R., Araldo, A., Akkinepally, A.P., Nahmias Biran, B.H., Basak, K., Seshadri, R., Deshmukh, N., Kumar, N., Azevedo, C.L., Ben-Akiva, M., 2018. Automated mobility-on-demand vs. mass transit: A multi-modal activity-driven agent-based simulation approach. Transportation Research Record: Journal of the Transportation Research Board (Online) .

Bazzani, A., Giorgini, B., Gallotti, R., Giovannini, L., Marchioni, M., Rambaldi, S., 2011. Towards congestion detection in transportation networks using gps data, in: 2011 IEEE Third International Conference on Privacy, Security, Risk and Trust and 2011 IEEE Third International Conference on Social Computing, IEEE. pp. 1455–1459.

Ben-Akiva, M., 2010. Planning and action in a model of choice, in: Choice Modelling: The State-of-the-Art and the State-of-Practice: Proceedings from the Inaugural International Choice Modelling Conference, Emerald Group Publishing Limited. pp. 19–34.

Ben-Akiva, M., Bowman, J.L., Gopinath, D., 1996. Travel demand model system for the information era. Transportation 23, 241–266.

Bischoff, J., Maciejewski, M., 2016. Simulation of city-wide replacement of private cars with autonomous taxis in berlin. Procedia computer science 83, 237–244.

Boesch, P.M., Ciari, F., Axhausen, K.W., 2016. Autonomous vehicle fleet sizes required to serve different levels of demand. Transportation Research Record 2542, 111–119.

Bösch, P.M., Becker, F., Becker, H., Axhausen, K.W., 2018. Cost-based analysis of autonomous mobility services. Transport Policy 64, 76–91.

Buisson, C., Ladier, C., 2009. Exploring the impact of homogeneity of traffic measurements on the existence of macroscopic fundamental diagrams. Transportation Research Record 2124, 127–136.

Burns, L., Jordan, W., Scarborough, B., 2015. Transforming personal mobility, the earth institute, columbia university.

Chen, T.D., Kockelman, K.M., Hanna, J.P., 2016. Operations of a shared, autonomous, electric vehicle fleet: Implications of vehicle & charging infrastructure decisions. Transportation Research Part A: Policy and Practice 94, 243–254.

Daganzo, C.F., 2007. Urban gridlock: Macroscopic modeling and mitigation approaches. Transportation Research Part B: Methodological 41, 49–62.

Daganzo, C.F., Gayah, V.V., , Gonzales, E.J.., 2011. Macroscopic relations of urban traffic variables: Bifurcations, multivaluedness and instability. Transportation Research Part B: Methodological 45, 278–288.

Daganzo, C.F., Geroliminis, N., 2008. An analytical approximation for the macroscopic fundamental diagram of urban traffic. Transportation Research Part B: Methodological 42, 771–781.

Ec.europa.eu, . Reducing co2 emissions from passenger cars. URL: `https://ec.europa.eu/clima/policies/transport/vehicles/cars_en`.

EPA, 2011. New Fuel Economy and Environment Labels for a New Generation of Vehicles (EPA-420-F-11-017). Technical Report.

Fagnant, D.J., Kockelman, K., 2015. Preparing a nation for autonomous vehicles: opportunities, barriers and policy recommendations. Transportation Research Part A: Policy and Practice 77, 167–181.

Fagnant, D.J., Kockelman, K.M., 2014. The travel and environmental implications of shared autonomous vehicles, using agent-based model scenarios. Transportation Research Part C: Emerging Technologies 40, 1–13.

Fagnant, D.J., Kockelman, K.M., 2018. Dynamic ride-sharing and fleet sizing for a system of shared autonomous vehicles in austin, texas. Transportation 45, 143–158.

Farhan, J., Chen, T.D., 2018. Impact of ridesharing on operational efficiency of shared autonomous electric vehicle fleet. Technical Report.

Fetene, G.M., 2014. A report on energy consumption and range of battery electric vehicles based on real-world driving data, in: Technical University of Denmark.

Gayah, V.V., Daganzo, C.F., 2011. Clockwise hysteresis loops in the macroscopic fundamental diagram: an effect of network instability. Transportation Research Part B: Methodological 45, 643–655.

Gayah, V.V., Gao, X.S., Nagle, A.S., 2014. On the impacts of locally adaptive signal control on urban network stability and the macroscopic fundamental diagram. Transportation Research Part B: Methodological 70, 255–268.

Geroliminis, N., Daganzo, C.F., 2008. Existence of urban-scale macroscopic fundamental diagrams: Some experimental findings. Transportation Research Part B: Methodological 42, 759–770.

Geroliminis, N., Daganzo, C.F., et al., 2007. Macroscopic modeling of traffic in cities, in: Transportation Research Board 86th Annual Meeting, No. 07-0413.

Geroliminis, N., Haddad, J., Ramezani, M., 2012. Optimal perimeter control for two urban regions with macroscopic fundamental diagrams: A model predictive approach. IEEE Transactions on Intelligent Transportation Systems 14, 348–359.

Geroliminis, N., Levinson, D.M., 2009. Cordon pricing consistent with the physics of overcrowding, in: Transportation and Traffic Theory 2009: Golden Jubilee. Springer, pp. 219–240.

Geroliminis, N., Sun, J., 2011. Hysteresis phenomena of a macroscopic fundamental diagram in freeway networks. Procedia-Social and Behavioral Sciences 17, 213–228.

Geroliminis, N., Zheng, N., Ampountolas, K., 2014. A three-dimensional macroscopic fundamental diagram for mixed bi-modal urban networks. Transportation Research Part C: Emerging Technologies 42, 168–181.

Godfrey, J., 1969. The mechanism of a road network. Traffic Engineering & Control 8.

Gonzales, E.J., Daganzo, C.F., 2012. Morning commute with competing modes and distributed demand: user equilibrium, system optimum, and pricing. Transportation Research Part B: Methodological 46, 1519–1534.

Haddad, J., Geroliminis, N., 2012. On the stability of traffic perimeter control in two-region urban cities. Transportation Research Part B: Methodological 46, 1159–1176.

Haddad, J., Ramezani, M., Geroliminis, N., 2013. Cooperative traffic control of a mixed network with two urban regions and a freeway. Transportation Research Part B: Methodological 54, 17–36.

Herman, R., Prigogine, I., 1979. A two-fluid approach to town traffic. Science 204, 148–151.

Hörl, S., Ruch, C., Becker, F., Frazzoli, E., Axhausen, K.W., 2019. Fleet operational policies for automated mobility: A simulation assessment for zurich. Transportation Research Part C: Emerging Technologies 102, 20–31.

Horni, A., Nagel, K., Axhausen, K.W., 2016. The multi-agent transport simulation MATSim. Ubiquity Press London.

Hyland, M., Mahmassani, H.S., 2018. Dynamic autonomous vehicle fleet operations: Optimization-based strategies to assign avs to immediate traveler demand requests. Transportation Research Part C: Emerging Technologies 92, 278–297.

Jadhav, A., 2018. Autonomous vehicle market by level of automation (level 3, level 4, and level 5) and component (hardware, software, and service) and application (civil, robo taxi, self-driving bus, ride share, self-driving truck, and ride hail) - Global opportunity analysis and industry forecast, 2019-2026. Technical Report.

Ji, Y., Luo, J., Geroliminis, N., 2014. Empirical observations of congestion propagation and dynamic partitioning with probe data for large-scale systems. Transportation Research Record 2422, 1–11.

Kass, R.E., 1990. Nonlinear regression analysis and its applications. Journal of the American Statistical Association 85, 594–596.

Katherine Kortum, M.N., 2018. National Academies - TRB Forum on Preparing for Automated Vehicles and Shared Mobility (Transportation Research Circular E-C236). Technical Report.

Keyvan-Ekbatani, M., Kouvelas, A., Papamichail, I., Papageorgiou, M., 2012. Exploiting the fundamental diagram of urban networks for feedback-based gating. Transportation Research Part B: Methodological 46, 1393–1403.

Kim, S., Tak, S., Yeo, H., 2018. Agent-based network transmission model using the properties of macroscopic fundamental diagram. Transportation Research Part C: Emerging Technologies 93, 79–101.

Kimeldorf, G.S., Wahba, G., 1970. A correspondence between bayesian estimation on stochastic processes and smoothing by splines. The Annals of Mathematical Statistics 41, 495–502.

Knoop, V.L., Hoogendoorn, S.P., 2013. Empirics of a generalized macroscopic fundamental diagram for urban freeways. Transportation research record 2391, 133–141.

Knoop, V.L., Van Lint, H., Hoogendoorn, S.P., 2015. Traffic dynamics: Its impact on the macroscopic fundamental diagram. Physica A: Statistical Mechanics and its Applications 438, 236–250.

Kouvelas, A., Saeedmanesh, M., Geroliminis, N., 2017. Enhancing model-based feedback perimeter control with data-driven online adaptive optimization. Transportation Research Part B: Methodological 96, 26–45.

Laris, M., . Uber and lyft concede they play role in traffic congestion in the district and other urban areas. URL: https://www.washingtonpost.com/transportation/2019/08/06/uber-lyft-concede-they-play-role-traffic-congestion-district-other-urban-areas/.

Laval, J.A., Castrillón, F., 2015. Stochastic approximations for the macroscopic fundamental diagram of urban networks. Transportation Research Part B: Methodological 81, 904–916.

Leclercq, L., Chiabaut, N., Trinquier, B., 2014. Macroscopic fundamental diagrams: A cross-comparison of estimation methods. Transportation Research Part B: Methodological 62, 1–12.

Leclercq, L., Geroliminis, N., 2013. Estimating mfds in simple networks with route choice. Procedia-Social and Behavioral Sciences 80, 99–118.

Leclercq, L., Parzani, C., Knoop, V.L., Amourette, J., Hoogendoorn, S.P., 2015. Macroscopic traffic dynamics with heterogeneous route patterns. Transportation Research Part C: Emerging Technologies 59, 292–307.

Leclercq, L., Sénécat, A., Mariotte, G., 2017. Dynamic macroscopic simulation of on-street parking search: A trip-based approach. Transportation Research Part B: Methodological 101, 268–282.

Lentzakis, A.F., Ware, S.I., Su, R., Wen, C., 2018. Region-based prescriptive route guidance for travelers of multiple classes. Transportation Research Part C: Emerging Technologies 87, 138–158.

Ligterink, N., 2017. Real-world Vehicle Emissions. Technical Report.

Loder, A., Ambühl, L., Menendez, M., Axhausen, K.W., 2017. Empirics of multi-modal traffic networks–using the 3d macroscopic fundamental diagram. Transportation Research Part C: Emerging Technologies 82, 88–101.

Lu, Y., Adnan, M., Basak, K., Pereira, F.C., Carrion, C., Saber, V.H., Loganathan, H., Ben-Akiva, M.E., 2015. Simmobility mid-term simulator: A state of the art integrated agent based demand and supply model, in: 94th Annual Meeting of the Transportation Research Board, Washington, DC.

Maciejewski, M., Bischoff, J., 2016. Congestion effects of autonomous taxi fleets .

Mahmassani, H., Williams, J.C., Herman, R., 1987. Performance of urban traffic networks, in: Proceedings of the 10th International Symposium on Transportation and Traffic Theory, Elsevier Science Publishing. pp. 1–20.

Mahmassani, H.S., Saberi, M., Zockaie, A., 2013. Urban network gridlock: Theory, characteristics, and dynamics. Transportation Research Part C: Emerging Technologies 36, 480–497.

Mariotte, G., 2018. Dynamic Modeling of Large-Scale Urban Transportation Systems. Ph.D. thesis.

Martinez, L.M., Viegas, J.M., 2017. Assessing the impacts of deploying a shared self-driving urban mobility system: An agent-based model applied to the city of lisbon, portugal. International Journal of Transportation Science and Technology 6, 13–27.

Mazloumian, A., Geroliminis, N., Helbing, D., 2010. The spatial variability of vehicle densities as determinant of urban network capacity. Philosophical Transactions of the Royal Society A: Mathematical, Physical and Engineering Sciences 368, 4627–4647.

Mühlich, N., Gayah, V.V., Menendez, M., 2014. An examination of mfd hysteresis patterns for hierarchical urban street networks using micro-simulation, in: 94th Annual Meeting of the Transportation Research Board.

Nagle, A.S., Gayah, V.V., 2013. A method to estimate the macroscopic fundamental diagram using limited mobile probe data, in: 16th International IEEE Conference on Intelligent Transportation Systems (ITSC 2013), IEEE. pp. 1987–1992.

OECD, 2018. Taxi, ride-sourcing and ride-sharing services. Technical Report.

Oh, S., Seshadri, R., Le, D.T., Zegras, P.C., Ben-Akiva, M.E., 2020a. Evaluating automated demand responsive transit using microsimulation. IEEE Access 8, 82551–82561.

Oh, S., Seshadri, R., Lima Azevedo, C., Kumar, N., Basak, K., Ben-Akiva, M., 2020b. Assessing the impacts of automated mobility-on-demand through agent-based simulation: A study of singapore (accepted). Transportation Research Part A: Policy and Practice .

Paipuri, M., Leclercq, L., 2020. Bi-modal macroscopic traffic dynamics in a single region. Transportation research part B: methodological 133, 257–290.

Pavone, M., Smith, S.L., Frazzoli, E., Rus, D., 2011. Load balancing for mobility-on-demand systems .

Ramezani, M., Haddad, J., Geroliminis, N., 2015. Dynamics of heterogeneity in urban networks: aggregated traffic modeling and hierarchical control. Transportation Research Part B: Methodological 74, 1–19.

Rayle, L., Dai, D., Chan, N., Cervero, R., Shaheen, S., 2016. Just a better taxi? a survey-based comparison of taxis, transit, and ridesourcing services in san francisco. Transport Policy 45, 168–178.

827 Saberi, M., Mahmassani, H.S., 2012. Exploring properties of networkwide flow–density rela-
828 tions in a freeway network. Transportation research record 2315, 153–163.

829 Saberi, M., Mahmassani, H.S., Hou, T., Zockaie, A., 2014. Estimating network fundamental
830 diagram using three-dimensional vehicle trajectories: Extending edie's definitions of traffic
831 flow variables to networks. Transportation Research Record 2422, 12–20.

832 Saeedmanesh, M., Geroliminis, N., 2015. Empirical observations of mfds and hysteresis loops
833 for multi-region urban networks with stop-line detectors. Technical Report.

834 Sakai, T., Bhavathrathan, B., Alho, A., Hyodo, T., Ben-Akiva, M., 2019. Modeling freight
835 generation, commodity contracts, and shipments for simmobility freight–a disaggregate
836 agent-based urban freight simulator, in: 98th Annual Meeting of the Transportation Re-
837 search Board.

838 Santi, P., Resta, G., Szell, M., Sobolevsky, S., Strogatz, S.H., Ratti, C., 2014. Quantifying
839 the benefits of vehicle pooling with shareability networks. Proceedings of the National
840 Academy of Sciences 111, 13290–13294.

841 Segui-Gasco, P., Ballis, H., Parisi, V., Kelsall, D.G., North, R.J., Busquets, D., 2019. Sim-
842 ulating a rich ride-share mobility service using agent-based models. Transportation 46,
843 2041–2062.

844 Seshadri, R., Kumarga, L., Atasoy, B., Danaf, M., Xie, Y., Azevedo, C., Zhao, F., Zegras, C.,
845 Ben-Akiva, M., 2019. Understanding preferences for automated mobility on demand using
846 a smartphone-based stated preference survey: a case study of singapore, in: Presented at
847 the Annual Meeting of the Transportation Research Board.

848 Shim, J., Yeo, J., Lee, S., Hamdar, S.H., Jang, K., 2019. Empirical evaluation of influential
849 factors on bifurcation in macroscopic fundamental diagrams. Transportation Research Part
850 C: Emerging Technologies 102, 509–520.

851 Shoufeng, L., Jie, W., van Zuylen, H., Ximin, L., 2013. Deriving the macroscopic fundamental
852 diagram for an urban area using counted flows and taxi gps, in: 16th International IEEE
853 Conference on Intelligent Transportation Systems (ITSC 2013), IEEE. pp. 184–188.

854 Simoni, M., Pel, A., Waraich, R., Hoogendoorn, S., 2015. Marginal cost congestion pricing
855 based on the network fundamental diagram. Transportation Research Part C: Emerging
856 Technologies 56, 221–238.

857 Simoni, M.D., Kockelman, K.M., Gurumurthy, K.M., Bischoff, J., 2019. Congestion pricing
858 in a world of self-driving vehicles: An analysis of different strategies in alternative future
859 scenarios. Transportation Research Part C: Emerging Technologies 98, 167–185.

860 Siyu, L., 2015. Activity-based Travel Demand Model: Application and Innovation. Ph.D.
861 thesis.

862 Smeed, R.J., 1967. The road capacity of city centers. Highway Research Record .

Spieser, K., Treleaven, K., Zhang, R., Frazzoli, E., Morton, D., Pavone, M., 2014. Toward a systematic approach to the design and evaluation of automated mobility-on-demand systems: A case study in singapore, in: Road vehicle automation. Springer, pp. 229–245.

Statista, 2017. Digital Market Outlook Segment Report. Technical Report.

Sun, L., Erath, A., 2015. A bayesian network approach for population synthesis. Transportation Research Part C: Emerging Technologies 61, 49–62.

Tsubota, T., Bhaskar, A., Chung, E., 2014. Macroscopic fundamental diagram for brisbane, australia: empirical findings on network partitioning and incident detection. Transportation Research Record 2421, 12–21.

Vazifeh, M.M., Santi, P., Resta, G., Strogatz, S., Ratti, C., 2018. Addressing the minimum fleet problem in on-demand urban mobility. Nature 557, 534.

WADA, K., AKAMATSU, T., HARA, Y., et al., 2015. An empirical analysis of macroscopic fundamental diagrams for sendai road networks. Interdisciplinary Information Sciences 21, 49–61.

Yildirimoglu, M., Ramezani, M., Geroliminis, N., 2015. Equilibrium analysis and route guidance in large-scale networks with mfd dynamics. Transportation Research Procedia 9, 185–204.

Zachariah, J., Gao, J., Kornhauser, A., Mufti, T., 2014. Uncongested mobility for all: A proposal for an area wide autonomous taxi system in New Jersey. Technical Report.

Zhang, R., Pavone, M., 2015. A queueing network approach to the analysis and control of mobility-on-demand systems, in: 2015 American Control Conference (ACC), IEEE. pp. 4702–4709.

Zhang, R., Pavone, M., 2016. Control of robotic mobility-on-demand systems: a queueing-theoretical perspective. The International Journal of Robotics Research 35, 186–203.

Zhang, W., Guhathakurta, S., Khalil, E.B., 2018. The impact of private autonomous vehicles on vehicle ownership and unoccupied vmt generation. Transportation Research Part C: Emerging Technologies 90, 156–165.

Zheng, N., Geroliminis, N., 2013. On the distribution of urban road space for multimodal congested networks. Procedia-Social and Behavioral Sciences 80, 119–138.

Zheng, N., Geroliminis, N., 2016. Modeling and optimization of multimodal urban networks with limited parking and dynamic pricing. Transportation Research Part B: Methodological 83, 36–58.

Zheng, N., Waraich, R.A., Axhausen, K.W., Geroliminis, N., 2012. A dynamic cordon pricing scheme combining the macroscopic fundamental diagram and an agent-based traffic model. Transportation Research Part A: Policy and Practice 46, 1291–1303.

CRediT authorship contribution statement

Simon Oh: Conceptualization, Methodology, Formal analysis, Software, Visualization, Writing - original draft, Funding acquisition. **Antonis F. Lentzakis:** Investigation, Formal analysis, Validation, Writing – review & editing. **Ravi Seshadri:** Conceptualization, Methodology, Validation, Writing – review & editing, Funding acquisition, Project administration. **Moshe Ben-Akiva**: Conceptualization, Methodology, Funding acquisition, Supervision.